University of Texas Rio Grande Valley

ScholarWorks @ UTRGV

2-2-2021

Scalable, cost-efficient synthesis and properties optimization of magnetoelectric cobalt ferrite/barium titanate composites

Farnaz Safi Samghabadi

Long Chang

Mohammad Khodadadi

Karen S. Martirosyan
The University of Texas Rio Grande Valley, karen.martirosyan@utrgv.edu

Dmitri Litvinov
University of Houston

Recommended Citation

Scalable, cost-efficient synthesis and properties optimization of magnetoelectric cobalt ferrite/barium titanate composites

Farnaz Safi Samghabadi, Long Chang, Mohammad Khodadadi, Karen S Martirosyan, and Dmitri Litvinov

COLLECTIONS

Paper published as part of the special topic on Magnetoelectric Materials, Phenomena, and Devices

View Online   Export Citation   CrossMark

ARTICLES YOU MAY BE INTERESTED IN

Strain-gradient effects in nanoscale-engineered magnetoelectric materials
APL Materials 9, 020903 (2021); https://doi.org/10.1063/5.0037421

Examination of possible high-pressure candidates of $SnTiO_3$: The search for novel ferroelectric materials
APL Materials 9, 021103 (2021); https://doi.org/10.1063/5.0029968

Ferroelectric field effect transistors: Progress and perspective
APL Materials 9, 021102 (2021); https://doi.org/10.1063/5.0035515

Scalable, cost-efficient synthesis and properties optimization of magnetoelectric cobalt ferrite/barium titanate composites

View Online   Export Citation   CrossMark

Farnaz Safi Samghabadi,[1] (ID) **Long Chang,**[2,3] (ID) **Mohammad Khodadadi,**[1,2] (ID) **Karen S Martirosyan,**[4] (ID) **and Dmitri Litvinov**[1,2,3,a)] (ID)

AFFILIATIONS

[1] Materials Science & Engineering, University of Houston, Houston, Texas 77204, USA
[2] Department of Electrical & Computer Engineering, University of Houston, Houston, Texas 77204, USA
[3] Center for Integrated Bio & Nano Systems, University of Houston, Houston, Texas 77204, USA
[4] Department of Physics and Astronomy, University of Texas Rio Grande Valley, Brownsville, Texas 78520, USA

Note: This paper is part of the Special Topic on Magnetoelectric Materials, Phenomena, and Devices.
[a)] Author to whom correspondence should be addressed: litvinov@uh.edu

ABSTRACT

Cobalt ferrite ($CoFe_2O_4$)/barium titanate ($BaTiO_3$) particulate composites exhibiting high magnetoelectric coefficients were synthesized from low-cost commercial precursors using mechanical ball milling followed by high-temperature annealing. $CoFe_2O_4$ (20 nm–50 nm) and either cubic or tetragonal $BaTiO_3$ nanoparticle powders were used for the synthesis. It was found that utilizing a 50 nm cubic $BaTiO_3$ powder as a precursor results in a composite with a magnetoelectric coupling coefficient value as high as 4.3 mV/Oe cm, which is comparable to those of chemically synthesized core–shell $CoFe_2O_4$–$BaTiO_3$ nanoparticles. The microstructure of these composites is dramatically different from the composite synthesized using 200 nm tetragonal $BaTiO_3$ powder. $CoFe_2O_4$ grains in the composite prepared using cubic $BaTiO_3$ powder are larger (by at least an order of magnitude) and significantly better electrically insulated from each other by the surrounding $BaTiO_3$ matrix, which results in a high electrical resistivity material. It is hypothesized that mechanical coupling between larger $CoFe_2O_4$ grains well embedded in a $BaTiO_3$ matrix in combination with high electrical resistivity of the material enhances the observed magnetoelectric effect.

INTRODUCTION

Magnetoelectric (ME) effect[1–5] has a number of promising applications in sensors, energy harvesting, magnetoelectric random access memory, antennas, drug delivery, etc.[6,7] In ME materials, the electric polarization can be controlled by varying the material's magnetization state, and conversely, varying the electric polarization affects the material's magnetization state. The ME effect has been observed in a few single-phase *multiferroic* materials; however, the effect is relatively weak at room temperature, which hampers useful applications. More robust ME behavior has been achieved in composites that combine mechanically coupled magnetostrictive and piezoelectric materials arranged in a matrix.[6,8] The ME effect in such composites is due to the induced stresses within the magnetostrictive or piezoelectric phases controlled by the application of external magnetic or electric fields, which transfer through the interface to the piezoelectric or magnetostrictive phases, respectively.[9] These composites can be produced in versatile connectivity configurations/matrices with a wide choice of materials, volume fractions, and microstructures[8,10] and can exhibit several orders of magnitude stronger ME effect than single-phase ME materials. Composite ME materials have been synthesized using a variety of techniques including sol–gel electrospinning of nanofibers,[9] polyol mediated process of composite ceramics,[10] molten-salt synthesis route for bulk composites,[11] core–shell structures,[12,13] wet ball-milling,[14] one-pot process,[15] carbon combustion synthesis,[16] and feather-like nanostructures.[17] The ME coefficient for these composites ranges from a few μV/Oe cm to several mV/Oe cm.[9] Core–shell

nanostructures, where the magnetostrictive core is fully enclosed by a piezoelectric shell, typically exhibit a higher value of ME coefficients. However, relatively complex chemical synthesis techniques along with the relatively low material yields limit their applications. Other synthesis approaches often suffer from poor interfaces between the two phases and/or low resistivity of magnetostrictive components, which hinders effective electrical poling.

In this study, the synthesis and characterization of $CoFe_2O_4$–$BaTiO_3$ particulate composites using dry ball-milling followed by annealing as a simple, low-cost, and highly reproducible powder processing method are presented. Cobalt ferrite, $CoFe_2O_4$, is a magnetostrictive material with magnetostriction coefficient values as high as 100 ppm–200 ppm at saturation,[18–20] and the tetragonal phase of barium titanate, $BaTiO_3$, is piezoelectric with reported d_{33} piezoelectric coefficient values in the 190 pC/N–260 pC/N range at room temperature.[21–25] The overarching goal of this work is to develop a scalable synthesis of an ME composite utilizing readily available commercial $CoFe_2O_4$ (CFO) and $BaTiO_3$ (BTO) precursor nanopowders. While there are several published reports on $CoFe_2O_4$–$BaTiO_3$ composites prepared by wet mechanical ball-milling, these reports have only partially explored the relationships between the process parameters and the properties of the composite.[14,26,27] The structural, magnetic, and ME properties of $CoFe_2O_4$–$BaTiO_3$ composites were investigated as functions of preparation conditions and the types of $BaTiO_3$ precursor nanoparticles used, namely, 50 nm cubic $BaTiO_3$ powder and 200 nm tetragonal $BaTiO_3$ powder. The ME coefficient in the optimized $CoFe_2O_4$–$BaTiO_3$ composite, where individual $CoFe_2O_4$ grains are fully enclosed by the $BaTiO_3$ matrix, was found to be comparable with the numbers reported for the composites based on core–shell structures.[28,29]

CoFe₂O₄–BaTiO₃ composite synthesis and sample conditioning

A 99.9% purity cobalt ferrite powder with 20 nm–50 nm particle sizes and 99.9% purity cubic and tetragonal barium titanate powders with 50 nm and 200 nm average particle sizes, respectively, were used in this study (see Fig. 1).[30] The composite mixture [$x \cdot CoFe_2O_4$–$(1 − x) \cdot BaTiO_3$, where x is the weight fraction] was prepared using mechanical ball milling. The mixture of $CoFe_2O_4$ and $BaTiO_3$ powders was ball-milled using a high-speed vibrating milling machine (MTI Corporation MSK-SFM-3) at 288 rpm for

5 h in a dry medium. Ball milling was performed using a nylon jar filled with zirconia balls with a ball to powder mass ratio of 10:1. The resulting mixture was pressed into pellets with a diameter of ~12 mm and a thickness of ~1 mm using a hydraulic press at a pressure of 120 bars. Next, the pellets were sintered in air for 4 h at 1200 °C in a tube furnace (MTI Corporation OTF-1200X-S).

Tetragonal $BaTiO_3$ is piezoelectric, but cubic $BaTiO_3$ does not exhibit ferroelectric behavior due to its centrosymmetric crystal structure. However, cubic $BaTiO_3$ undergoes a structural transformation as it reaches certain critical temperatures. The most typical conversion from paraelectric cubic to ferroelectric tetragonal crystal structure occurs through cooling through its Curie point at 120 °C. This structural transformation is due to a slight displacement of Ti^{4+} cations with respect to the anion center along the crystallographic c axis.[21–23]

The annealed pellets were electrically poled in the direction perpendicular to the pellet surface in a heated silicone oil bath at 150 °C, which is above the $BaTiO_3$ Curie temperature for 15 min. The poling voltage was maintained after the pellet was removed from the bath for an additional 15 min as the pellet cools down to room temperature. As discussed later, the magnitude of the poling voltage affects the measured ME properties.

Materials characterization

The magnetoelectric behavior was evaluated using a custom-built ME characterization system similar to the one described in the literature.[31–33] The opposing surfaces of the samples were coated with a thin layer of conductive silver paste (MG chemicals 842-AR silver print) as the electrical contacts for magnetoelectric measurement. The ac ME voltage across the pellet induced by the ac magnetic field (1 Oe at 1 KHz) superimposed over a dc magnetic field is recorded as a function of dc magnetic field, which can be swept between −7 kOe and 7 kOe. Stimulating the sample with an ac magnetic field superimposed to the dc magnetic field eliminates the contribution of charges accumulated in the grain boundaries and defects in the material during the poling process into the ME signal.[33–35] Piezo-force microscopy (PFM) measurements were performed utilizing an MFP-3D Origin+ (Asylum Research-Oxford Instruments) atomic force microscope in the Dual AC Resonance Tracking (DART) mode using a silicon tip coated with Ti/Ir (5/20). The microstructure was examined utilizing an FEI Dual Beam 235 Focused Ion Beam instrument. The magnetostriction
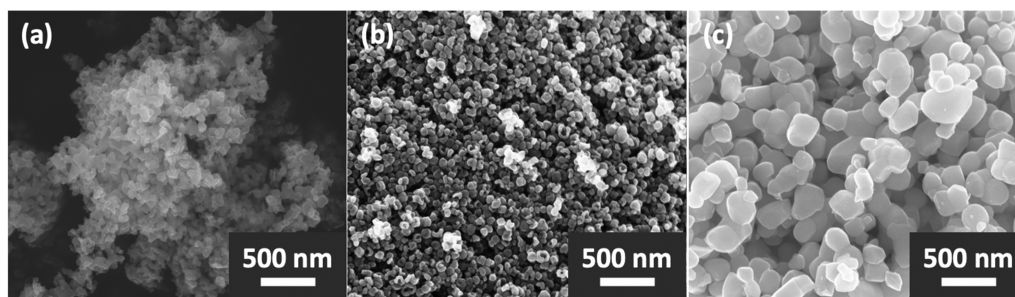

FIG. 1. SEM images of (a) 20 nm–50 nm $CoFe_2O_4$, (b) 50 nm cubic $BaTiO_3$, and (c) 200 nm tetragonal $BaTiO_3$.

measurement was performed using a linear strain gauge (Micro-Measurements C2A-06-062LW-350) mounted on the surface of the pellets using a commercial bonding kit (Micro-Measurements MMF006678/M-BOND-200), and the data were acquired through a DAQ device (Micro-Measurements MM01-350) with a built-in Wheatstone quarter-bridge circuit. The magnetic properties of the samples were characterized using a LakeShore (model 735) vibrating sample magnetometer (VSM). All the magnetic measurements were conducted in a transversal (field lines perpendicular to the plane of the pellet) configuration at ambient temperature. The crystal structure of the composites was studied using a Rigaku Smartlab x-ray diffractometer with Cu–kα radiation (λ = 1.540 60 Å). The data were collected in the range of $20 < 2\theta < 80$ with a step size of $0.01°$ and a scan step time of 1 s and analyzed using X'Pert HighScore software.

RESULTS AND DISCUSSION

Two factors play a crucial role in the effectiveness of the ferroic phase conjugation: resistivity of the ceramic, which directly governs the electrical poling effectiveness, and the interface of the two materials, which influences the strain transfer.[36] As discussed above, the $CoFe_2O_4$ pellets were conditioned prior to the measurements through electric poling to optimize ME properties. Due to the finite resistivity of the $CoFe_2O_4$ phase in the composite and the leakage currents through a network of electrically interconnected

$CoFe_2O_4$ grains, there are limitations on the magnitude of the electric field that can be applied across the pellet. The dependence of the maximum achievable electric field that was applied during the poling (before samples get damaged by local Joule heating) and the corresponding resistivity values of the samples at the poling temperature (150 °C, see above) on $CoFe_2O_4$ content and the type of $BaTiO_3$ precursor (cubic or tetragonal) are shown in Fig. 2(a). Since $BaTiO_3$ is an insulator, higher $BaTiO_3$ content leads to better electrical isolation of $CoFe_2O_4$ grains and the increase in pellet resistance, which, in turn, enables higher poling voltages. To measure the maximum achievable ME coefficient value for a given composition of the composite, the maximum achievable electric field was applied to each sample during electric poling. Furthermore, the values of the ME coefficient resulting from poling under identical conditions were compared. For these measurements, an electric field of 0.8 kV/cm was used, which is the maximum achievable electric field for the composite with the lowest resistivity (using the cubic $BaTiO_3$ precursor). The ME response as a function of dc magnetic field for $x \cdot CoFe_2O_4$–$(1 − x) \cdot BaTiO_3$ composites prepared with two different types of $BaTiO_3$ precursors and poled with the highest dc voltage applicable depending on their resistivity is shown in Figs. 2(b) and 2(c). All the curves exhibit hysteretic behavior[10,28] that originates from the hysteretic nature of the magnetization reversal in $CoFe_2O_4$. A comparison of the maximum ME coefficient of the pellets prepared and conditioned differently is shown in Fig. 2(d). The cubic samples produce higher ME coefficients than the
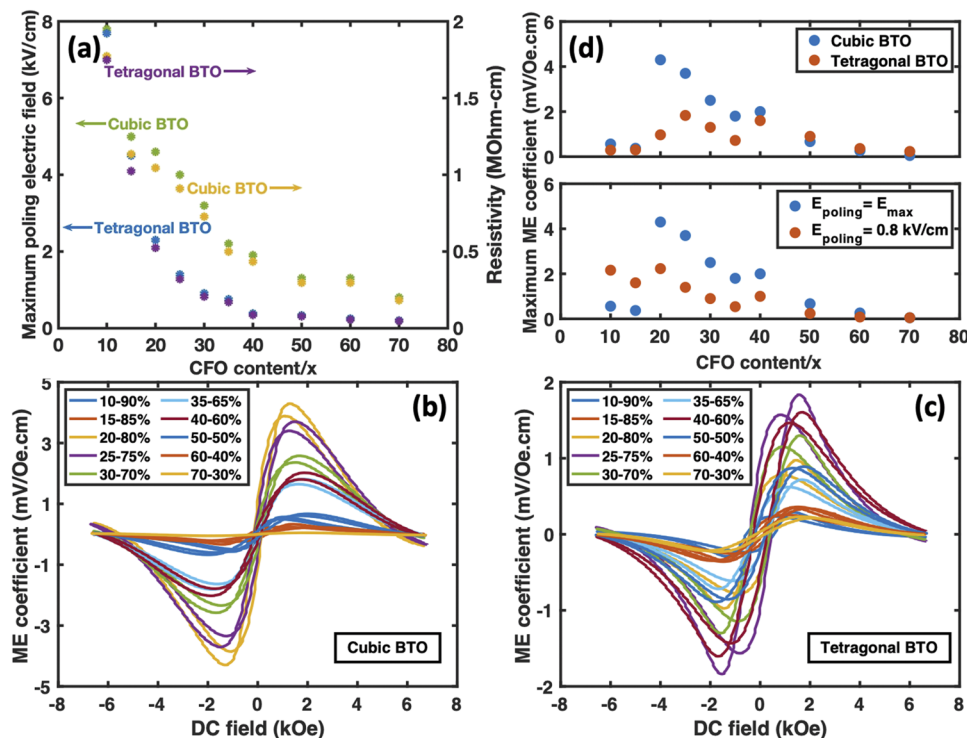

FIG. 2. (a) Correlation of maximum poling electric field and resistivity with $CoFe_2O_4$ content in $CoFe_2O_4$ composites, ME coefficient as a function of dc magnetic field for different compositions prepared with (b) cubic and (c) tetragonal $BaTiO_3$ precursors, (d) maximum ME coefficient vs $CoFe_2O_4$ content in different composites depending on the $BaTiO_3$ precursor type (top) and magnitude of the poling electric field applied to cubic samples (bottom).

tetragonal samples when the concentration of $CoFe_2O_4$ is below 50%. The highest ME coefficient is achieved at a $CoFe_2O_4$:$BaTiO_3$ concentration of 20%–80% for cubic samples (4.3 mV/Oe cm) and 25%–75% for tetragonal samples (1.83 mV/Oe cm). When the samples based on cubic $BaTiO_3$ precursor were poled at the same electric fields (0.8 kV/cm), the ME coefficient of each composite is reduced, but their relative performance remains approximately the same. The samples were prepared multiple times to verify these trends.

Piezo-Force Microscopy (PFM) images of $0.3CoFe_2O_4$–$0.7BaTiO_3$ composites are shown in Fig. 3. These samples were polished to a mirror finish (rms roughness below 10 nm) using progressively higher grit sandpaper followed by polishing paste. The PFM probe is placed in contact with the sample surface. Upon applying a 5 V ac driving voltage to the probe, the piezoelectric domains in the sample respond by straining, which leads to the deflection of the cantilever. This deflection is interpreted as piezo-amplitude and piezo-phase images that exhibit a contrast between piezoelectric $BaTiO_3$ and non-piezoelectric $CoFe_2O_4$ materials. The images show $CoFe_2O_4$ grains (darker regions on PFM amplitude and phase scans) within a $BaTiO_3$ matrix (lighter regions), as the brighter domains have higher piezoresponse and a different phase compared to dark regions. The variations in the PFM amplitude observed for $BaTiO_3$ grains result from the variations of crystallographic orientation of individual grains with respect to the excitation electric field, properties of surrounding grains, individual grain sizes, residual stresses, etc. The characteristic grain sizes observed in the sample prepared using cubic $BaTiO_3$ powder are significantly larger than the grain sizes in the sample prepared using tetragonal $BaTiO_3$ powder [see Figs. 3(b) and 3(e)], which is the result of significant differences in the morphologies and

compositions of $BaTiO_3$/$CoFe_2O_4$ precursor mixtures that affect the grain growth dynamics.[37–41]

Due to the better isolation of $CoFe_2O_4$ grains in cubic samples compared to the networked $CoFe_2O_4$ grains in tetragonal ones, they can be poled more efficiently. Moreover, the formation of a higher interfacial area or core–shell-like structure between piezomagnetic and piezoelectric phases in samples prepared with cubic $BaTiO_3$ precursor facilitates the strain transfer between two phases.

SEM images of $0.3CoFe_2O_4$–$0.7BaTiO_3$ samples for the cases of cubic and tetragonal $BaTiO_3$ precursors are shown in Figs. 4(a) and 4(b), respectively. To distinguish between $CoFe_2O_4$ and $BaTiO_3$ phases, the samples were etched in hydrochloric acid (HCl 50% v/v aqueous solution) for 3 h to selectively remove $CoFe_2O_4$. The resulting SEM images of HCl etched $0.3CoFe_2O_4$–$0.7BaTiO_3$ samples for the cases of cubic and tetragonal $BaTiO_3$ precursors are shown in Figs. 4(b) and 4(e), respectively. Focused ion-beam (FIB) cross-sectioning was used to reveal the depth profile of the composite microstructure. It should be noted that material damage due to Ga ion implantation during typical FIB cross-sectioning used in this work is limited to ~20 nm penetration depth, which is significantly smaller than the characteristic length scales probed here.[42] As shown in Fig. 4(f), the voids (dissolved $CoFe_2O_4$) in the samples based on tetragonal $BaTiO_3$ precursors extend up to 8 μm below the surface of the sample. Since the pores (etched away $CoFe_2O_4$) are observed all the way down to 8 μm below the surface, $CoFe_2O_4$ grains in the tetragonal $BaTiO_3$ precursor based samples are fairly well interconnected. On the other hand, the FIB cross section of the sample based on cubic $BaTiO_3$ precursor reveals that individual $CoFe_2O_4$ grains are physically isolated from each other (by $BaTiO_3$) since no voids are observed below the sample surface [see Fig. 4(c)]. This is
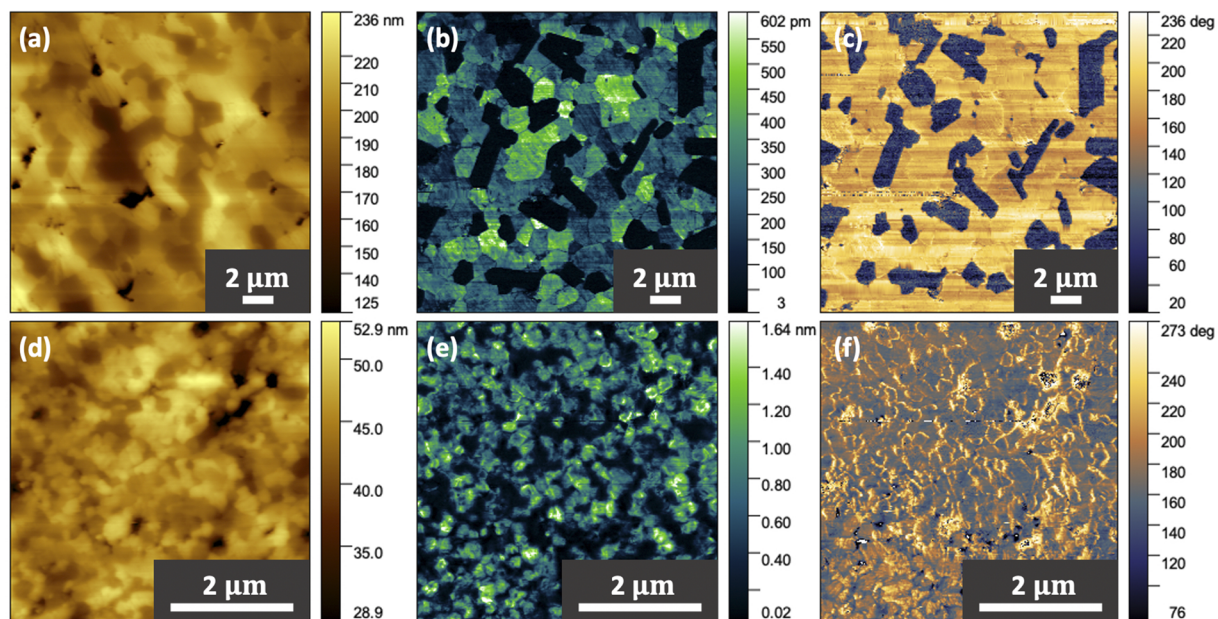

FIG. 3. PFM imaging of $0.3CoFe_2O_4$–$0.7BaTiO_3$ composites prepared with cubic (top row) and tetragonal (bottom row) $BaTiO_3$ precursors: [(a) and (d)] height (surface topography), [(b) and (e)] PFM amplitude, and [(c) and (f)] PFM phase.
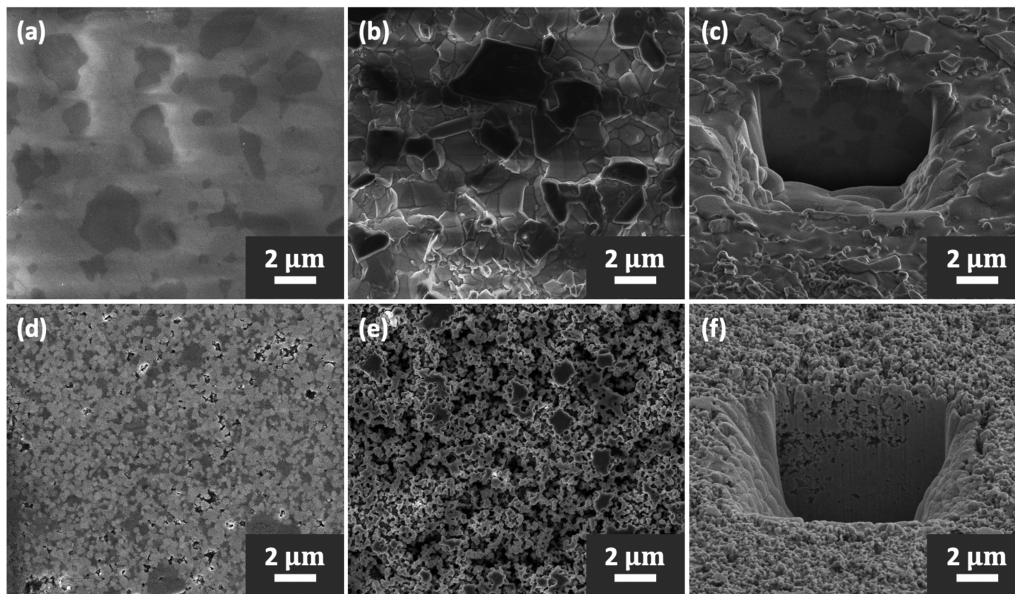
FIG. 4. SEM images of polished 0.3CoFe$_2$O$_4$–0.7BaTiO$_3$ composites (cubic: top and tetragonal BaTiO$_3$: bottom row): [(a) and (d)] surface, [(b) and (e)] etched surface, and [(c) and (f)] FIB-etched cross section.

in agreement with lower resistance observed in tetragonal precursor samples as compared to cubic ones.

The dependence of magnetostriction, λ, and piezomagnetic coefficient, $d\lambda/dH$, on the magnitude of applied dc magnetic field

for 0.3CoFe$_2$O$_4$–0.7BaTiO$_3$ composite prepared with two types of BaTiO$_3$ is shown in Figs. 5(a) and 5(b), respectively. The composite synthesized with the cubic BaTiO$_3$ precursor exhibits lower magnetostriction values compared to the tetragonal BaTiO$_3$ precursor
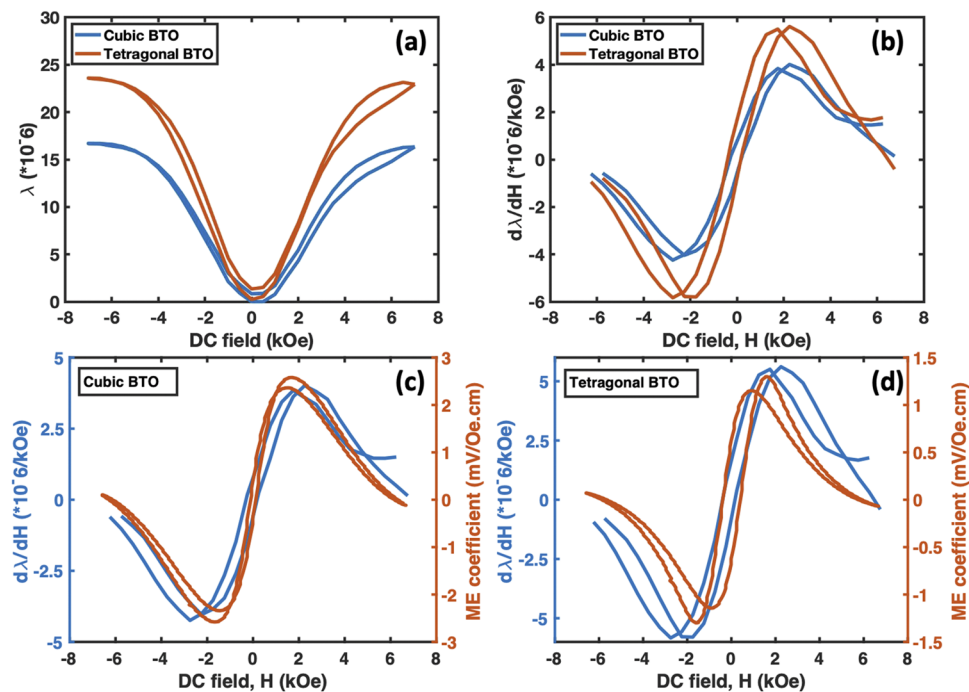

FIG. 5. (a) Comparison of magnetostriction, λ, as a function of DC magnetic field in 0.3CoFe$_2$O$_4$–0.7BaTiO$_3$ composites, (b) comparison of the derivative of magnetostriction, and [(c) and (d)] comparison of the derivative of magnetostriction and ME coefficient for cubic and tetragonal composites, respectively.
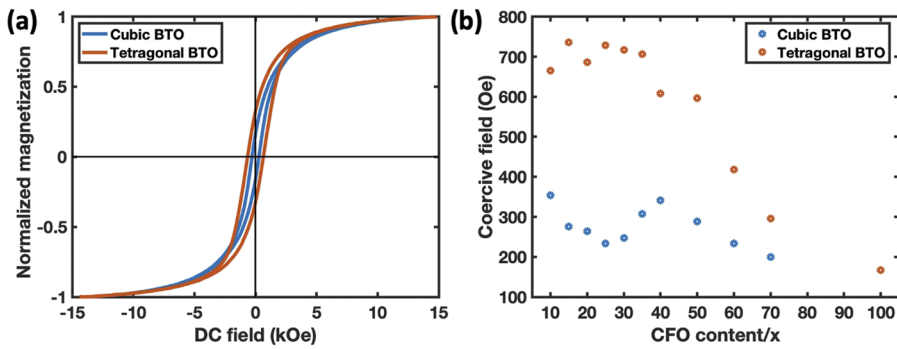
FIG. 6. (a) M–H loop of $0.3CoFe_2O_4$–$0.7BaTiO_3$ composites and (b) variation of coercivity with $CoFe_2O_4$ proportion in the composite.

based samples. This is attributed to the finer microstructure and smaller $CoFe_2O_4$ grain sizes in tetragonal $BaTiO_3$ samples that help to more effectively distribute the strain throughout the composite.[18] It should be noted that the coercivity values are the same in the magnetic field dependencies of the ME coefficient, magnetostriction, and magnetization (see Fig. 6).[43,44]

The dependence of the magnetoelectric coefficient on several materials properties can be approximately described using the following equation:[45]

$$\alpha_{ME} = x(1-x) \cdot \frac{d\lambda}{dH} \cdot \frac{d_{33}}{\varepsilon_{r33}} \cdot Y_{33}, \tag{1}$$

where x is the volume fraction of the magnetostrictive component, $d\lambda/dH$ is the piezomagnetic coefficient, d_{33} is the piezoelectric coefficient, ε_{r33} is the relative permittivity of the composite, and Y_{33} is Young's modulus. The above equation is a relatively crude approximation; however, it aids in the interpretation of the trends observed in experimental data. According to Eq. (1), the magnetoelectric coefficient, α_{ME}, is proportional to the value of piezomagnetic coefficient, $d\lambda/dH$, at a given dc magnetic field, which is consistent with the respective data shown in Figs. 5(c) and 5(d).[32,34] Although the piezomagnetic coefficient is higher for $CoFe_2O_4$–$BaTiO_3$ composites based on the tetragonal $BaTiO_3$ precursor, it does not result in higher magnetoelectric coefficient values, as shown in Fig. 2. The value of the magnetoelectric coefficient is affected by a higher dielectric constant due to the lower resistivity of tetragonal $BaTiO_3$ based composites [see Eq. (1)], limitations to effectively pole the composites (again due to low resistivity),
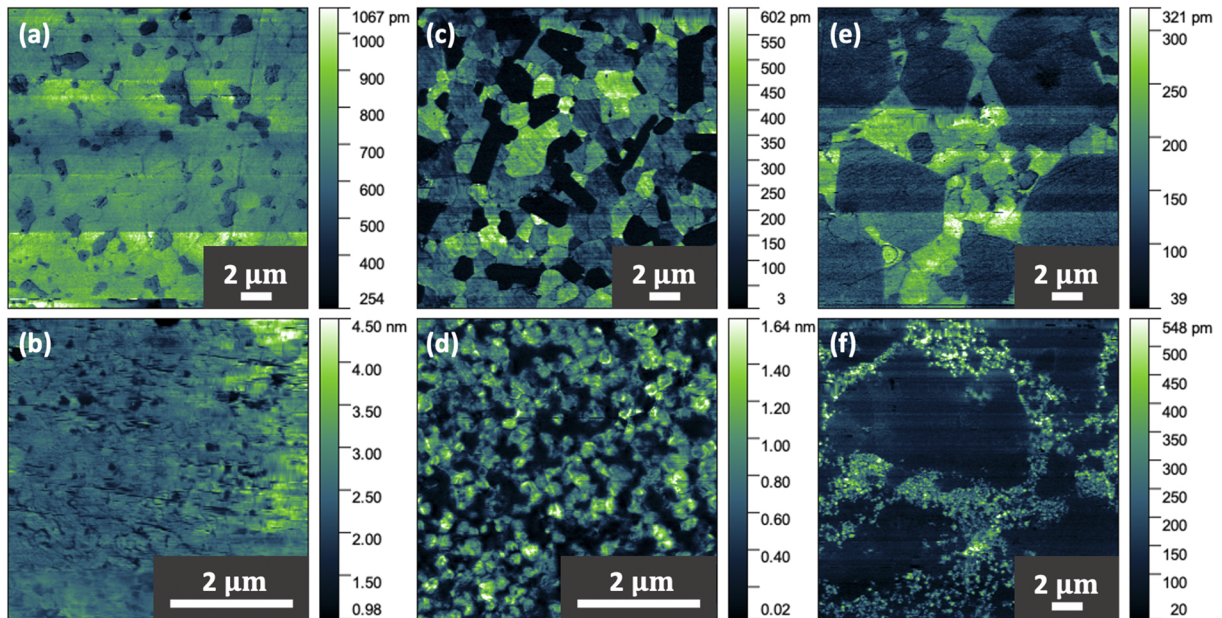

FIG. 7. Comparison of PFM amplitude scans of $CoFe_2O_4$–$BaTiO_3$ composites prepared with cubic (top row) and tetragonal (bottom row) $BaTiO_3$ precursors for $CoFe_2O_4$–$BaTiO_3$ composites: [(a) and (b)] 10%–90%, [(c) and (d)] 30%–70%, and [(e) and (f)] 70%–30%.
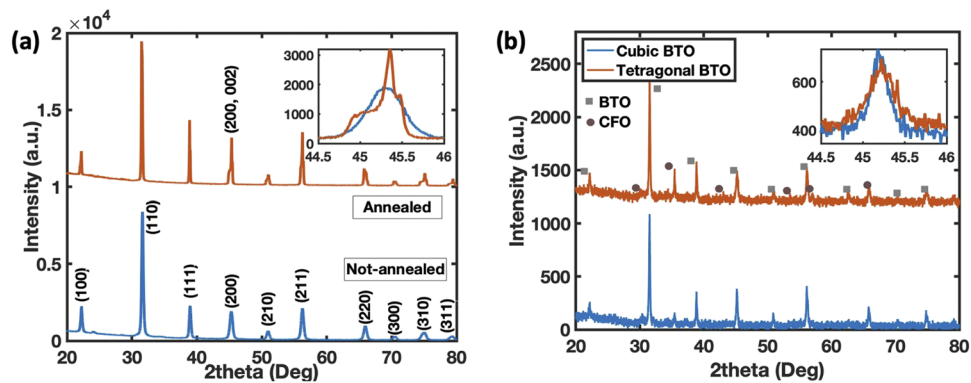
FIG. 8. X-ray diffraction patterns of (a) cubic BaTiO$_3$ before and after annealing at 1200 °C and (b) annealed 0.3CoFe$_2$O$_4$–0.7BaTiO$_3$ composites. The inset shows the BaTiO$_3$ (200) reflection.

and a variety of other factors including significant microstructural differences.

The M–H loops for 0.3CoFe$_2$O$_4$–0.7BaTiO$_3$ composites and the dependence of their coercivity on CoFe$_2$O$_4$ content are shown in Figs. 6(a) and 6(b), respectively. The magnetic field was applied perpendicular to the pellet surface. The observation of the lower coercivity values in samples prepared using the cubic BaTiO$_3$ precursor is consistent with the above observation that CoFe$_2$O$_4$ grain size in these samples is significantly larger than CoFe$_2$O$_4$ grain size in samples prepared using the tetragonal BaTiO$_3$ precursor. The large CoFe$_2$O$_4$ grain size (>1 μm) facilitates magnetization reversal processes via domain wall motion resulting in lower coercivity values.

PFM amplitude scans shown in Fig. 7 for samples prepared cubic and tetragonal BaTiO$_3$ precursors illustrate the increase in the characteristic CoFe$_2$O$_4$ grain sizes [dark regions with zero (or near zero) PFM amplitude correspond to CoFe$_2$O$_4$ grains] with the increase in CoFe$_2$O$_4$ content in the CoFe$_2$O$_4$–BaTiO$_3$ composite. Similarly to the above observations of coercivity value differences between samples prepared cubic and tetragonal BaTiO$_3$ precursors, the increase in CoFe$_2$O$_4$ grain size for higher CoFe$_2$O$_4$ content samples leads to the reduction of the composite coercivity. This is also consistent with previously published reports.[46–48]

The XRD spectra of cubic BaTiO$_3$ before and after annealing at 1200 °C for 4 h are shown in Fig. 8(a). Non-annealed cubic BaTiO$_3$ holds Pm-3m space group (JCPDS data No.: 01-074-1961) with the calculated lattice parameters of a = b = c = 3.9966 Å.[49–51] While characteristic peaks of tetragonal BaTiO$_3$ are observed for the annealed powder and indexed with P4mm space group (JCPDS No.: 01-081-2201) with lattice parameters of a = b = 3.9961 Å and c = 4.03 219 Å. The estimated tetragonality factor (c/a) is 1.009, which is close to the bulk value of 1.011. The XRD spectra of 0.3CoFe$_2$O$_4$–0.7BaTiO$_3$ samples after annealing are shown in Fig. 8(b). The two patterns do not exhibit peak splitting at 45° corresponding to the Miller index of (200) and (002) as expected for the tetragonal crystal structure. This can be attributed to the peak broadening of nano-crystalline particles or the cubic-dominant structure, which leads to the lower tetragonality factor.[52,53] However, as demonstrated in this work, the

composite samples based on both cubic and tetragonal precursors do exhibit magnetoelectric properties, which confirms the presence of tetragonal BaTiO$_3$ in the composite.

CONCLUSIONS

In summary, magnetoelectric composites of CoFe$_2$O$_4$–BaTiO$_3$ were synthesized using commercial CoFe$_2$O$_4$ and BaTiO$_3$ precursors and an inexpensive and scalable process based on ball-milling and high-temperature sintering/annealing. It was observed that magnetoelectric properties are strongly affected by the CoFe$_2$O$_4$–BaTiO$_3$ composition, where the highest magnetoelectric coefficient is exhibited in samples prepared from a 20% CoFe$_2$O$_4$/80% BaTiO$_3$ precursor mixture. The effect of size and crystal structure of the BaTiO$_3$ nanoparticle precursor on magnetoelectric and related magnetic properties of the CoFe$_2$O$_4$–BaTiO$_3$ composite was investigated. Higher magnetoelectric coupling coefficients comparable to those of core–shell nanostructures were observed for composites prepared with 50 nm cubic BaTiO$_3$. Microstructural characterization using SEM and PFM revealed that CoFe$_2$O$_4$ grains in a composite based on cubic BaTiO$_3$ precursor nanoparticles are larger and better isolated from each other by the surrounding BaTiO$_3$ matrix than CoFe$_2$O$_4$ grains in a composite based on tetragonal BaTiO$_3$ precursor nanoparticles. Larger, higher crystallinity magnetostrictive (CoFe$_2$O$_4$) and piezoelectric (BaTiO$_3$) phases likely result in enhanced magnetostrictive and piezoelectric coefficients; the enhanced interfaces between the phases improve the coupling between the phases; and higher electrical resistivity enables more effective poling and leads to the effective reduction of the relative permittivity. Combining these effects results in higher ME coefficient values that are observed in the optimized composite based on cubic BaTiO$_3$ powders.

DATA AVAILABILITY

The data that support the findings of this study are available from the corresponding author upon reasonable request.

REFERENCES

[1] N. A. Spaldin, S.-W. Cheong, and R. Ramesh, Phys. Today **63**(10), 38 (2010).

[2] J. Ma, J. Hu, Z. Li, and C.-W. Nan, Adv. Mater. **23**, 1062 (2011).

[3] J. S. Andrew, J. D. Starr, and M. A. K. Budi, Scr. Mater. **74**, 38 (2014).

[4] D. C. Lupascu, H. Wende, M. Etier, A. Nazrabi, I. Anusca, H. Trivedi, V. V. Shvartsman, J. Landers, S. Salamon, and C. Schmitz-Antoniak, GAMM-Mitteilungen **38**, 25 (2015).

[5] J.-M. Hu, L.-Q. Chen, and C.-W. Nan, Adv. Mater. **28**, 15 (2016).

[6] Y. Cheng, B. Peng, Z. Hu, Z. Zhou, and M. Liu, Phys. Lett. A **382**, 3018 (2018).

[7] H. Palneedi, V. Annapureddy, S. Priya, and J. Ryu, Actuators **5**, 9 (2016).

[8] N. Ortega, A. Kumar, J. F. Scott, and R. S. Katiyar, J. Phys.: Condens. Matter **27**, 504002 (2015).

[9] A. Baji, Y.-W. Mai, R. Yimnirun, and S. Unruan, RSC Adv. **4**, 55217 (2014).

[10] T. Walther, U. Straube, R. Köferstein, and S. G. Ebbinghaus, J. Mater. Chem. C **4**, 4792 (2016).

[11] J. Nie, G. Xu, Y. Yang, and C. Cheng, Mater. Chem. Phys. **115**, 400 (2009).

[12] M. Etier, Y. Gao, V. V. Shvartsman, D. C. Lupascu, J. Landers, and H. Wende, in Proceedings of the ISAF-ECAPD-PFM 2012, 2012.

[13] G. V. Duong, R. Groessinger, and R. S. Turtelli, IEEE Trans. Magn. **42**, 3611 (2006).

[14] A. Khamkongkaeo, P. Jantaratana, C. Sirisathitkul, T. Yamwong, and S. Maensiri, Trans. Nonferrous Met. Soc. China **21**, 2438 (2011).

[15] S. Q. Ren, L. Q. Weng, S.-H. Song, F. Li, J. G. Wan, and M. Zeng, J. Mater. Sci. **40**, 4375 (2005).

[16] C. T. D. Leo, C. T. De Leo, G. C. Dannangoda, M. A. Hobosyan, J. T. Held, F. Safi Samghabadi, M. Khodadadi, D. Litvinov, K. A. Mkhoyan, and K. S. Martirosyan, Ceram. Int. **47**(4), 5415–5422 (2021).

[17] Y. Deng, J. Zhou, D. Wu, Y. Du, M. Zhang, D. Wang, H. Yu, S. Tang, and Y. Du, Chem. Phys. Lett. **496**, 301 (2010).

[18] S. D. Bhame and P. A. Joy, Sens. Actuators, A **137**, 256 (2007).

[19] S. D. Bhame and P. A. Joy, J. Am. Ceram. Soc. **91**, 1976 (2008).

[20] A. Muhammad, R. Sato-Turtelli, M. Kriegisch, R. Grössinger, F. Kubel, and T. Konegger, J. Appl. Phys. **111**, 013918 (2012).

[21] B. Jiang, L. Iocozzia, L. Zhao, H. Zhang, Y.-W. Harn, Y. Chen, and Z. Lin, Chem. Soc. Rev. **48**, 1194 (2019).

[22] M. Acosta, N. Novak, V. Rojas, S. Patel, R. Vaish, J. Koruza, G. A. Rossetti, and J. Rödel, Appl. Phys. Rev. **4**, 041305 (2017).

[23] A. Filippetti and N. A. Hill, Phys. Rev. B **65**, 195120 (2002).

[24] B. Ertug, Am. J. Eng. Res. **2**(8), 1–7 (2013).

[25] L. Simon-Seveyrat, A. Hajjaji, Y. Emziane, B. Guiffard, and D. Guyomar, Ceram. Int. **33**, 35 (2007).

[26] R. Kumar, S. Guha, R. K. Singh, and M. Kar, J. Magn. Magn. Mater. **465**, 93 (2018).

[27] M. Rasly, M. Afifi, A. E. Shalan, and M. M. Rashad, Appl. Phys. A **123**, 331 (2017).

[28] G. V. Duong and R. Groessinger, J. Magn. Magn. Mater. **316**, e624 (2007).

[29] G. V. Duong, R. S. Turtelli, and R. Groessinger, J. Magn. Magn. Mater. **322**, 1581 (2010).

[30] US Research Nanomaterials, Inc., https://www.us-nano.com/. Stock numbers US3843, US3835, and US3828, respectively.

[31] M. M. Kumar, M. Mahesh Kumar, A. Srinivas, S. V. Suryanarayana, G. S. Kumar, and T. Bhimasankaram, Bull. Mater. Sci. **21**, 251 (1998).

[32] G. V. Duong, R. Groessinger, M. Schoenhart, and D. Bueno-Basques, J. Magn. Magn. Mater. **316**, 390 (2007).

[33] J. V. Vidal, A. A. Timopheev, A. L. Kholkin, and N. A. Sobolev, Nanostructures and Thin Films for Multifunctional Applications (Springer, Cham, 2016).

[34] J. Paul Praveen, V. R. Monaji, S. Dinesh Kumar, V. Subramanian, and D. Das, Ceram. Int. **44**, 4298 (2018).

[35] D. Damjanovic, The Science of Hysteresis (Academic Press, 2006), p. 337.

[36] M. Fiebig, ChemInform **36**, R123 (2005).

[37] A. Rollett, G. S. Rohrer, and J. Humphreys, Recrystallization and Related Annealing Phenomena (Newnes, 2017).

[38] M. N. Kelly, W. Rheinheimer, M. J. Hoffmann, and G. S. Rohrer, Acta Mater. **149**, 11 (2018).

[39] S. J. Dillon, M. Tang, W. C. Carter, and M. P. Harmer, Acta Mater. **55**, 6208 (2007).

[40] R. D. MacPherson and D. J. Srolovitz, Nature **446**, 1053 (2007).

[41] J.-S. Park, "Microstructural evolution and control in the directional solidification of Fe-C-Si alloys," Ph.D. dissertation (Iowa State University, 1990).

[42] J. Mayer, L. A. Giannuzzi, T. Kamino, and J. Michael, MRS Bull. **32**, 400 (2007).

[43] E. Hristoforou and A. Ktena, J. Magn. Magn. Mater. **316**, 372 (2007).

[44] M. M. Vopson, Y. K. Fetisov, G. Caruntu, and G. Srinivasan, Materials **10**, 963 (2017).

[45] A. S. Zubkov, Elektrichestvo **10**, 77 (1978).

[46] M. M. El-Okr, M. A. Salem, M. S. Salim, R. M. El-Okr, M. Ashoush, and H. M. Talaat, J. Magn. Magn. Mater. **323**, 920 (2011).

[47] R. S. Yadav, I. Kuřitka, J. Vilcakova, J. Havlica, J. Masilko, L. Kalina, J. Tkacz, J. Švec, V. Enev, and M. Hajdúchová, Adv. Nat. Sci.: Nanosci. Nanotechnol. **8**, 045002 (2017).

[48] O. Perales-Pérez and Y. Cedeño-Mattei, Magnetic Spinels: Synthesis, Properties and Applications (IntechOpen, 2017).

[49] Y. Kobayashi, A. Nishikata, T. Tanase, and M. Konno, J. Sol-Gel Sci. Technol. **29**, 49 (2004).

[50] K. Uchino, E. Sadanaga, and T. Hirose, J. Am. Ceram. Soc. **72**, 1555 (1989).

[51] X. Li and W.-H. Shih, J. Am. Ceram. Soc. **80**, 2844 (1997).

[52] H.-W. Lee, S. Moon, C.-H. Choi, and D. K. Kim, J. Am. Ceram. Soc. **95**, 2429 (2012).

[53] X. Zhu, Z. Zhang, J. Zhu, S. Zhou, and Z. Liu, J. Cryst. Growth **311**, 2437 (2009).